

Title: Epithelial repair is a two-stage process driven first by dying cells and then by their neighbours.

Dorothy Kuipers^{1,2}, Aida Mehonic³, Mihoko Kajita⁴, Loïc Peter^{5,6}, Yasuyuki Fujita⁴, Tom Duke^{3,5}, Guillaume Charras^{5,7,*}, Jonathan E. Gale^{2,7,*}.

¹CoMPLEX PhD program, University College London, Gower Street, London, WC1E 6BT, UK

²UCL Ear Institute, University College London, 332 Gray's Inn Road, London, WC1X 8EE, UK

³Department of Physics and Astronomy, University College London, Gower Street, London, WC1E 6BT, UK

⁴Division of Molecular Oncology, Institute for Genetic Medicine, Hokkaido University, Sapporo, Hokkaido, Japan

⁵London Centre for Nanotechnology, University College London, 17-19 Gordon Street, London, WC1H 0AH, UK

⁶Ecole Centrale Paris, Grande Voie des Vignes, 92295 Châtenay-Malabry, France

⁷Department of Cell and Developmental Biology, University College London, Gower Street, London, WC1E 6BT, UK

*Authors for correspondence: Jonathan Gale (j.e.gale@ucl.ac.uk) or Guillaume Charras (g.charras@ucl.ac.uk). These authors contributed equally to this work.

Running Title: Dying epithelial cells drive their own extrusion

Summary

Epithelial cells maintain an essential barrier despite continuously undergoing mitosis and apoptosis. Biological and biophysical mechanisms have evolved to remove dying cells whilst maintaining that barrier. Cell extrusion is thought to be driven by a multicellular filamentous actin ring formed by the neighbouring cells, with its contraction providing the mechanical force for extrusion, with little or no contribution from the dying cell. We use live confocal imaging, providing time-resolved 3D observations of actomyosin dynamics to reveal new mechanical roles for dying cells in their own extrusion from monolayers. Dying cell clearance could be subdivided into two-stages. The first, previously unidentified, stage was driven by the dying cell, which exerted tension on its neighbours through the action of a cortical contractile F-actin and myosin ring at the cell apex. The second stage, consistent with previous studies, was driven by a multicellular F-actin ring in the neighbouring cells that moved from the apical to the basal plane to extrude the dying cell. Critically, these data reinstate the dying cell as an active physical participant in cell extrusion rather than an innocent bystander.

Introduction

An essential role of epithelial tissues is to form a tight barrier that prevents the passage of cells, macromolecules, and solutes across the epithelium (Marchiando et al., 2010). In developing and mature tissues, under both physiological and patho-physiological conditions, epithelial cell death continuously occurs and therefore a variety of mechanisms have evolved to remove dead or dying cells whilst preserving barrier integrity. In intestinal epithelia, division and differentiation of stem cells gives rise to a constant flux of cells from the crypts to the villus tips where individual cells are extruded (Madara, 1990; Potten and Loeffler, 1990). In inner ear sensory epithelia, cell divisions are relatively rare but after a damaging event non-sensory supporting cells scission dying the apical surfaces of hair cells, releasing the apical parts into the lumen (Bird et al., 2010). In cultured epithelial monolayers, dying cells can be extruded from the epithelium either apically (Rosenblatt et al., 2001) or basally (Slattum et al., 2009) and the latter has been proposed as a possible cause for cancer progression (Marshall et al., 2011). Recently, cell extrusion has also been shown to play a fundamental role in tissue homeostasis (Eisenhoffer and Rosenblatt, 2013), and in both developing and mature tissues,

overcrowding is relieved by extruding extranumerary cells (Eisenhoffer et al., 2012; Marinari et al., 2012).

The molecular mechanisms underlying cell extrusion have been the focus of much attention. A seminal study reported that cell extrusion is driven by a multicellular filamentous actin (F-actin) ring formed within the cells surrounding the dying cell (Rosenblatt et al., 2001). Following induction of cell death by UV-exposure, a signal emanates from the dying cell through sphingosine-1-phosphate (Gu et al., 2011). Immunostaining studies and live imaging studies of wound healing after single-cell ablation within monolayers have revealed that this signal then leads to the formation of a multicellular F-actin ring that originates at the monolayer apex (Gu and Rosenblatt, 2012; Rosenblatt et al., 2001; Tamada et al., 2007). Subsequently, myosin is recruited to the intercellular junction of surrounding cells in a process dependent upon p115-RhoGEF, rho-kinase, and GTPases of the rho family (Rosenblatt et al., 2001; Slattum et al., 2009; Tamada et al., 2007). The multicellular ring descends basally and, once at the base of the monolayer, lamellipodial protrusions originating from the neighbouring cells join below the dying cell reforming intercellular junctions that extrude the dead cell (Tamada et al., 2007). Based on these studies, the current consensus is that the dying cell provides a biochemical signal for its neighbours but plays no mechanical role in extrusion (Andrade and Rosenblatt, 2011; Cai and Sheetz, 2009; Gu and Rosenblatt, 2012). However, detailed time-resolved observations of actomyosin dynamics during cell extrusion are lacking, making a thorough understanding of the biological and biophysical mechanisms of extrusion impossible.

Here, using live 3-D imaging, we examined F-actin and myosin dynamics underlying cell extrusion from cultured monolayers over the entire duration of the process. In contrast to previous studies, we identified distinct roles for both the dying cell and its neighbours. We show that removal of dying cells is a multi-step process involving distinct stages of actomyosin activity. The initial stage involving an increase in actomyosin contractility in the dying cell has not previously been reported.

Results

A multistep process leads to cell extrusion in UV-treated monolayers

Previous studies have relied on exposure of epithelial monolayers to UV to induce cell death (Gu et al., 2011; Marshall et al., 2011; Rosenblatt et al., 2001; Slattum et al., 2009). Although this is a robust experimental protocol, all of the cells are exposed to the stimulus and eventually die. This makes long-term observation of single-cell extrusion events challenging, because neighbouring cells often die within tens of minutes of one another. To overcome these limitations, we placed a custom-made mask in the epifluorescence light-path of a microscope to expose individual cells within confluent MDCK-monolayers to UV and selectively induce cell death. We combined this technique with 3-D live imaging to follow the cellular processes leading to cell extrusion.

Live imaging of extrusion within confluent lifeact-GFP MDCK-monolayers revealed that the removal of dying cells involved multiple phases of F-actin dynamics occurring in different focal planes (**Figure 1**, **Movie 1**). During the initial phase, a rosette formed at the monolayer apex cleaving the dying cell and enclosing most of its body within the epithelium. This phase involved F-actin activity at the monolayer apex. In the apical plane, the intercellular junctions around the dying cell closed inwards over the course of 15-30 minutes (**Figure 1a**). Simultaneously, the surrounding cells spread towards the centre of the dying cell enclosing it and forming a multi-cellular rosette visible in the apical plane. This process led to bulging of the apex of the dying cell at the surface of the monolayer before scission as a result of junctional closure. The remainder of the cell body was enclosed within the monolayer. This “scission” phase was observed in all cell death events (48/48 cells, 12 experiments). At the onset of rosette formation, strong F-actin enrichment in the shape of a ring was visible at the apical contacts between healthy cells and the dying cell (**Figure 1a**). Closure of this apical ring occurred horizontally in a single z-plane with a steady speed of $0.2 \pm 0.1 \mu\text{m} \cdot \text{min}^{-1}$ (18 cells, 4 experiments, **Figure 1b and S1a**, **Movie 2**).

In the second phase, the apical F-actin ring moved basally around the dying cell over 30-40 minutes, leading to extrusion from the monolayer (**Figure 1c**). As soon as the F-actin ring reached the basal plane, the aspect of the F-actin-enriched zone changed from ring-like to lamellipodial-like (**Figure S1b**). Over the next 60-90min the neighbouring cells crawled underneath the dying cell, in a process resembling the later stages in cell ablation experiments (Tamada et al., 2007) and see Figure 5. This extrusion stage was observed in all death events that occurred in cells surrounded by healthy neighbours

(17/17 cells, 8 experiments). However, in cases in which one or several surrounding cells also died, extrusion was not observed. These data suggest that the neighbouring cells were necessary for the process and acted collectively to bring about extrusion. Overall, F-actin activity observed during extrusion in the present experiments supports the multi-cellular F-actin ring mechanism proposed to drive the extrusion of dying cells (Rosenblatt et al., 2001) and wound healing of epithelia at both the single-cell (Tamada et al., 2007) and tissue level (Martin and Lewis, 1992). Hence, our observations revealed that the extrusion of dying cells is a multistep process taking ~2.5h to complete from the initial movement of the cell-cell junctions (**Figure 1d**). Only part of this process had previously been described, therefore we investigated the acto-myosin dynamics underlying extrusion.

Cell membranes do not permeabilise until extrusion is complete

To gain insight into the relative timing of cell death and extrusion, we determined when membrane permeabilisation occurred by including propidium iodide (PI, a membrane-impermeant nucleic acid probe) in the imaging medium. We also determined when phosphatidyl serine appeared on the outer leaflet of the plasma membrane by including AlexaFluor633-tagged annexin-V (an early death signal (Fadok et al., 1998)). During apical contraction and rosette formation, no PI or annexin-V labeling were observed in dying cells (45/45 cells from 4 experiments and 8/8 cells from 3 experiments respectively, **Figure 2a**). In contrast, cells that had been fully extruded had both strong annexin and PI labeling (10/10 cells, 3 experiments, **Figure 2b**), in agreement with (Rosenblatt et al., 2001). These data indicated that the integrity of dying cells remained uncompromised during the initial apical contraction stage and that membrane permeabilization only occurred once extrusion was complete. This sequence of events contrasts with single-cell laser wounding experiments, where permeabilisation precedes F-actin ring formation (Tamada et al., 2007).

An F-actin ring is present in dying cells but not in surrounding cells during apical contraction and enclosure

To distinguish F-actin activity in dying cells from that in surrounding cells we used monolayers formed by mixing MDCK cells stably expressing either mRFP-actin or lifeAct-GFP (**Figure 3a**). By live-imaging in locations where dying cells expressed a different fluorophore from its neighbours, it was possible to definitively identify whether the F-actin enrichment observed during initial apical contraction was localized in the

dying or surrounding cells. During rosette formation, scission, and enclosure, a uniform F-actin enrichment was observed at the cortex of the dying cell in the apical plane consistent with previous work (Rosenblatt et al., 2001) (**Figure 3b**, **Movie 3**, 11/11 cells, 4 experiments). This F-actin ring contracted inwards over 15-30 min concurrent with junctional closure (**Figure 3b** and **Movie 3**), apparently driving self-scission and occurring considerably faster than reported previously (Rosenblatt et al., 2001). Simultaneously, less-organised F-actin activity was observed in the basal plane of the dying cell (**Figure 3b**, **Movie 4**), perhaps reflecting loss of focal adhesions. Crucially, there was little evidence of F-actin enrichment in the surrounding cells in any plane during this initial phase, in contrast to previous descriptions (Rosenblatt et al., 2001) (**Figure 3c**, **Movie 5**, 9/9 cells, 4 experiments). At the apical surface, neighbouring cells moved inwards synchronously with apical contraction of the dying cell (**Figure 3d**, $t=0-35$ minutes, **Movies 6 & 7**). In the absence of an F-actin ring in the surrounding cells, this suggested that, at this stage, they were pulled inwards by the contractile ring in the dying cell, perhaps via the tight junctions that remained intact during cell removal (**Figure 4a**). Immunostaining of monolayers fixed 2h after UV-exposure revealed the presence of strong cortical F-actin enrichment located inside the tight junctions between the dying cell and its neighbours (**Figure 4a**). Together, the data from fixed specimens, live-imaging data, and the lack of membrane permeabilisation during this new initial phase suggests that an F-actin ring within the dying cell drives rosette formation by pulling neighbouring cells inwards.

Extrusion involves F-actin activity in the neighbouring cells

During the latter phase of cell extrusion, F-actin enrichment appeared in the surrounding cells at the monolayer apex, forming a multicellular ring encircling the dying cell (**Figure 3d**, 45min, and **Figure S1b**). This multicellular ring then moved basally, following the contour of the dying cell (**Figure 3d**, 40-60min, **Movies 6 & 7**). During this time, cortical F-actin enrichment persisted at the apex of the dying cell (**Movies 1 & 6**). Once the multicellular F-actin ring reached the basal plane, F-actin-rich protrusions extended beneath the dying cell, consistent with the lamellipodial crawling described in wound healing experiments (Martin and Lewis, 1992; Tamada et al., 2007). This sequence occurred in all extrusions imaged to completion (6/6 cells, 4 experiments). In monolayer samples fixed 2.5h after UV-exposure, multicellular F-actin rings were clearly visible outside of the tight-junctions between dying cells and their neighbours (**Figure 4b**).

Overall, F-actin dynamics during the latter extrusion phase were consistent with the multicellular F-actin rings described in single cell laser ablation experiments (Tamada et al., 2007) and in cell extrusion in UV-treated monolayers (Gu et al., 2011; Marshall et al., 2011; Rosenblatt et al., 2001; Slattum et al., 2009).

The dynamics of extrusion reflect those observed in single-cell wound healing experiments

In our experiments, ~75min separated the initial movement of intercellular junctions at the monolayer apex from the arrival of the multicellular F-actin ring in the basal plane, far longer than reported (20min) in single-cell wound healing experiments (Tamada et al., 2007). We hypothesized that the slower overall dynamics were due to our inclusion and the occurrence of an initial apical contraction and enclosure phase not observed during single-cell wound healing experiments. To test this, we observed F-actin dynamics during single-cell wound healing under conditions identical to our UV experiments. Following laser-ablation, the cell's membrane was immediately permeabilized and a multicellular F-actin ring was formed around the ablated cell. This ring then descended towards the basal plane while contracting over the course of 30min (16 cells, 4 experiments, **Figure 5**). This behaviour was in all aspects identical to a previous report (Tamada et al., 2007) and its duration was very similar to that of the extrusion phase in our UV-induced cell death experiments. Based on its duration and characteristic F-actin dynamics, we propose that the multicellular extruding F-actin ring reported in single-cell wound healing (Tamada et al., 2007) is equivalent to the multicellular F-actin ring we observe during the extrusion of dying cells in UV-exposed monolayers.

Active myosin co-localises with the F-actin ring and myosin activity is required during apical contraction and enclosure

Having identified this new, earlier event in cell extrusion, we investigated a potential role for myosin contraction in generating the mechanical forces underlying this phase. First, we imaged UV-exposed MDCK-cell monolayers stably expressing myosin regulatory light chain-(MRLC)-GFP. Prior to any detectable evidence of cell death, MRLC-GFP fluorescence was cytoplasmic, with a slight enrichment at the basal plane in focal adhesions (0 min, **Figure 6a** and [Movie 8](#)). Simultaneous with the onset of apical contraction, myosin relocated within the dying cell to form a distinct ring in the same plane as the F-actin ring (5-10min, **Figure 6a** and [Movie 8](#)). As rosette formation

progressed, myosin fluorescence increased correlating with the F-actin enrichment noted in lifeact-GFP cells (16/16 cells, 4 experiments, **Figure 1a-b**). To determine whether the increase in myosin fluorescence intensity resulted from additional recruitment or concentration of already bound protein over a smaller area, we tracked the apical junctions surrounding the dying cell during rosette formation and measured total junctional MRLC fluorescence intensity. Between the onset of junctional movement and the completion of apical contraction, intensity of MRLC-GFP increased 5 ± 3 fold (6 cells, 3 experiments), indicating that the observed increase in myosin fluorescence represented protein recruitment. Furthermore, immunostaining of MDCK-monolayers fixed 2h after UV-exposure revealed enrichment in phosphorylated myosin light chain (pMLC) at the cortex of dying cells (**Figure 6b**).

To determine if myosin contraction was necessary to drive rosette formation during the apical contraction phase, we imaged live UV-exposed monolayers stably expressing lifeact-Ruby in the presence of the myosin-II ATPase inhibitor blebbistatin. At low blebbistatin concentrations (10-25 μ M), rosette formation began normally but, once the ring contracted to 50-75% of the initial cell diameter, contraction stopped and the dying cell lost its junctional actin ring and detached from the substrate leaving an epithelial “hole” (16/16 cells, 4 experiments, **Figure 6c**, [Movie 9](#)). Simultaneous with loss of the junctional actin ring, the intercellular junctions surrounding the cell relaxed to their initial positions. Live imaging with PI confirmed membrane permeabilisation along with the tearing apart of the dying cell. In addition, the observed partial apical closure took 30 ± 12 min (n=16), ~2-fold slower than controls and a duration normally sufficient for complete rosette formation in control conditions. With 100 μ M blebbistatin, we could not detect any evidence of F-actin ring formation or junctional closure. Instead, the dying cell either disintegrated or appeared to be torn apart by its neighbours in the absence of any contraction and this process was accompanied by membrane permeabilisation (22/22 cells, 3 experiments, **Figure 6d**). These data showed that myosin contraction was necessary for successful rosette formation.

Rho-mediated contractility in the dying cell drives the apical contraction phase of cell removal

Next, we sought to determine which of the dying or the surrounding cells provided the motile force for the progression of the initial apical contraction phase. Previous work has

shown that, during the process that we have identified as the later extrusion phase, active RhoA is necessary in the neighbouring cells but not in the dying cell (Rosenblatt et al., 2001). Immunostaining of monolayers fixed 2h after UV-exposure revealed that, during the apical-contraction phase, dying cells displayed strong RhoA-GTP staining (**Figure 7a**). This suggested that increases in RhoA activity may drive the observed increase in myosin contractility (**Figure 6a and b**).

We therefore investigated the role of RhoA activity during the apical contraction phase. To distinguish between activity in the dying cell and its neighbours, we used mosaics of lifeact-GFP-MDCK cells and MDCK cells in which RhoA activity was inhibited by doxycycline-induced expression of the catalytic domain of p50-RhoGAP tagged with mCherry (**Figure 7b-c**). First, we verified that high RhoGAP expression correlated with reduced RhoA-GTP labelling in MDCK cells showing that RhoGAP expression was able to reduce RhoA-GTP levels (**Figure S2**). A similar effect was noted with pMLC staining in MDCK cells expressing p50-RhoGAP (**Figure S3**). Next, we examined how RhoGAP expression affected the two phases of cell clearance. In MDCK-monolayer mosaics, dying wild-type lifeact-GFP cells could still drive rosette formation and undergo self-scission even when the majority of their neighbours were RhoGAP-positive (5/5 cells from 3 experiments, **Figure 7b**, **Movie 10**). Furthermore, rosette morphology was unperturbed at junctions with RhoGAP-positive cells. In contrast, in 50% of cases, dying RhoGAP-positive cells with a majority of lifeact-GFP neighbours could not complete rosette formation or scission, a phenotype observed with low blebbistatin concentrations (6/12 cells, 5 experiments, **Figure 6c**, **7c**, **Movie 11**). These data suggest that in our experiments induction of RhoGAP expression only led to a partial, rather than a total reduction in myosin activity in dying cells. The remaining cells were able to drive normal rosette formation, perhaps via caspase-mediated rho-kinase activation (Coleman et al., 2001; Sebbagh et al., 2001) or due to an insufficient reduction in RhoA activity by p50-RhoGAP expression (**Figure S2**). Together, these experiments indicated that RhoA-mediated myosin contractility in the dying cell was necessary to drive the initial apical contraction phase of cell extrusion and that, during this phase, the contribution of neighbouring cells was minimal.

Numerical simulations suggest that the apical contraction phase can be driven by the dying cell alone

Our experimental observations indicated that, during the apical contraction phase, the dying cell provided the mechanical force for rosette formation through a ~5-fold increase in myosin localization to its apical cortex that, we assumed, resulted in a proportional increase in contractility. To verify this hypothesis and explore alternate biophysical mechanisms leading to rosette formation, we developed a simple numerical simulation of the monolayer apex using a vertex model (Farhadifar et al., 2007; Marinari et al., 2012). Based on uniform cortical-localization of myosin throughout apical contraction, we assumed that all cortical tension could be represented by a single contractility term Γ acting over the cell perimeter. In our model, cells possessed an area elastic modulus K arising from limited cell volume compressibility, a contractility Γ arising from cortical myosin activity, and intercellular adhesion A acting at cell-cell junctions. The model was carefully calibrated to represent mechanical equilibrium in monolayer-epithelia growing on glass (see **Materials and Methods**). We carried out numerical experiments in which, at time $t=0$, we changed the physical properties of either the dying cell (A_D , Γ_D , K_D), its immediate neighbours (A_N , Γ_N , K_N), or both the dying cell and its neighbours. From these, we determined the combinations of physical changes that could in principle drive rosette formation (defined here as a >80% reduction in the apical area of the dying cell).

Changes in the dying cell's adhesion to its neighbours A_D alone could not drive rosette formation (**Figure 8a-b**). Changes in the dying cell's elasticity K_D alone could only drive rosette formation if K_D was reduced to zero at the onset of rosette formation (**Figure 8a, Figure 8b**, $K_D=0$ and $0.5K$). In our experiments, the preservation of membrane integrity (**Figure 2a**) and the presence of a well-defined F-actin cytoskeleton in the dying cells (**Figure 3b**) suggest that their elasticity *is not* reduced to zero. Furthermore, measurements of cell elasticity during cell death report either increases in elasticity (Kim et al., 2012) or decreases (at most 75%) of cellular elasticity during cell death (Kim et al., 2012; Wang and Pelling, 2010), suggesting that rosette formation through reduction of K_D to zero *does not* occur during apoptosis. In contrast, a five-fold increase in the contractility Γ_D of the dying cell, comparable to our live-imaging of myosin, was sufficient alone to generate a rosette (**Figure 8b**, $\Gamma_D=5\bar{\Gamma}$). Interestingly, a partial decrease in dying cell elasticity K_D coupled with complete loss of adhesion to neighbours A_D could also drive rosette formation (**Figure 8b**, $A_D=0$, $K_D=0.3$). Whilst a decrease in elastic modulus K_D during cell death has been reported in some conditions (Wang and Pelling, 2010), complete loss

of adhesion between the dying cell and its neighbours A_D is in contradiction with our experimental observations (**Figures 3 and 4**) and previous work showing that the barrier function of monolayers is maintained during extrusion (Rosenblatt et al., 2001). Changes in the neighbouring cells alone or in combination with changes in the dying cell could in theory also give rise to rosette formation. Indeed, rosettes could be obtained through moderate increases in the adhesion of neighbouring cells to one another A_N , combined or not with decreases in the adhesion between the surrounding cells and the dying cell A_D (**Figure 8b**, $A_N=4A$ and $A_N=3A$ with $A_D=0$). Although an increase in the elasticity K_N of neighbouring cells has been suggested to drive extrusion of transformed cells from epithelia, even a 100-fold increase in K_N , far greater than measured experimentally (Hogan et al., 2009), was insufficient to drive rosette formation in our model, perhaps signifying that extrusion of transformed cells may occur through mechanisms different to that of dying cells (**Figure 8b**, $K_N=100K$).

Discussion

In this study, we captured the cellular and cytoskeletal changes leading to the extrusion of dying cells with high spatio-temporal accuracy and critically, we revealed new mechanical roles for dying cells in their own extrusion. Indeed, clearance of dying cells could be subdivided into two-stages based on the location of actomyosin activity (**Figure 8c**). The first, previously unidentified, stage was driven by the dying cell which exerted tension on its neighbours through a cortical contractile F-actin ring resulting in formation of a cellular-rosette at the epithelial surface. The second stage was driven by a *multicellular* F-actin ring in the neighbouring cells that moved apico-basally to extrude the dying cell, consistent with previous studies (Rosenblatt et al., 2001; Tamada et al., 2007).

The apical contraction and enclosure phase involved formation of apical rosettes through assembly of a contractile cortical actomyosin ring downstream of RhoA in the dying cell. Live-imaging of mosaics of cells expressing F-actin markers tagged with different fluorophores together with immunostaining data provided definitive localization of the contractile F-actin ring within the dying cell during this initial phase. Apical contraction of the dying cell was accompanied by enrichment in total myosin (5-fold) and a clear increase in pMLC. This coincided with scission of the dying cell, with cell's apex being shed and the remaining cell body being enclosed within the monolayer. Apical ring closure required myosin contractility downstream of RhoA in the dying cell as

myosin-inhibition and expression of the catalytic domain of p50RhoGAP in the dying cell both resulted in failure of rosette formation. These results contrasted with the extrusion observed in crowding-induced delamination in the *drosophila notum*, where rosette formation around the delaminating cell is driven by increased myosin contractility in the surrounding cells (Marinari et al., 2012). The present data suggest an altruistic role for the dying cell during cell extrusion (Andrade and Rosenblatt, 2011; Mills et al., 1999). Cortical F-actin enrichment in the dying cell has been observed in MDCK-monolayers but the authors concluded that it did not participate in extrusion based on the lack of effect of C3-toxin (a RhoA/RhoC/cdc42 inhibitor) injected into the dying cell (Rosenblatt et al., 2001). However, in that study dying cells were selected for injection morphologically using phase contrast microscopy and thus, *ipso facto* were likely to have already completed the initial apical contraction phase.

Why is an initial phase of apoptotic cell extrusion driven by increased contractility of the dying cell necessary if the later extrusion phase can proceed in its absence, i.e. as in single-cell wound healing experiments (Tamada et al., 2007)? One simple explanation is that the initial phase is an altruistic act by the dying cell to trigger its own effective extrusion, while ensuring preservation of the monolayer's barrier function. The initial phase may harness the increase in contractility that is concomitant with cell death to bring intercellular junctions into position to seal the barrier and scission part of the cell to facilitate extrusion, before triggering assembly of a contractile multicellular F-actin ring in its neighbours (Eisenhoffer et al., 2012; Gu et al., 2011). Another intriguing possibility is that contractility and rosette formation during the initial phase provides an essential mechanical signal to the surrounding cells by transiently increasing junctional tension and local cellular density. This could perhaps activate molecular mechanisms similar to those involved in cell extrusion in response to overcrowding in epithelia (Eisenhoffer et al., 2012). Future work will be necessary to precisely determine how each phase contributes to overall extrusion, what signals coordinate the transition from the initial apical-contraction phase to the extrusion phase, and whether basal extrusion is the result of a defective extrusion by the surrounding cells.

Our computational simulations of the apical contraction phase indicated that increases in myosin contractility F_D in the dying cell alone were sufficient to drive rosette formation. Interestingly, an increase in adhesion A_N of surrounding cells to one another could also drive rosette formation, something that should manifest itself as an increase in cadherin

recruitment to intercellular junctions between the surrounding cells. Further work will be necessary to determine if and to what extent, an increase in intercellular adhesion between surrounding cells also contributes to rosette formation. Finally, the physical processes underlying the extrusion phase still remain unclear and 3-D computational models explicitly modelling the apical area, basal adhesion, and lateral junctions are required to gain the necessary physical insight to tackle this.

Materials and methods

Cell culture

Madin-Darby Canine Kidney II (MDCK) cells were maintained at 37°C/5% CO₂ in Dulbecco's Modified Eagle Medium (DMEM) with 10% fetal calf serum and 1% penicillin/streptomycin. MDKC-expression mosaics were created by mixing cell-lines expressing proteins tagged with different fluorophores in a 1:10 ratio before plating.

Generation of cell lines

MDCK-cell lines stably expressing fluorescent markers for F-actin and myosin (actin-mRFP and MRLC-GFP) were generated as described in (Charras et al., 2006). Lifeact-GFP and lifeact-ruby (Riedl et al., 2008) were gifts from R. Wedlich-Soldner (MPI, Martinsried). Retroviruses generation and cell subcloning are described in (Harris et al., 2012). To establish MDCK cells stably expressing mCherry-p50RhoGAP catalytic domain in a tetracycline-inducible manner, MDCK-pTR cells (Hogan et al., 2009) were transfected with pcDNA/TO/mCherry-p50RhoGAP catalytic domain (Hogan et al., 2009), followed by selection in medium containing 5µg.ml⁻¹ of blasticidin (Invitrogen) and 400µg.ml⁻¹ of zeocin (Invitrogen). Cells were then subcloned to obtain a monoclonal cell line with an epithelial phenotype.

Inducing cell death of individual cells by UV-exposure

Cells were exposed to UV light for 3 minutes in a Stratalinker1800 to induce cell death (Rosenblatt et al., 2001). For the majority of live-imaging experiments an aluminium mask with eight holes (1.5mm apart) was placed in the epifluorescence light-path of a microscope resulting in ~10µm diameter illumination spots (75µm apart) on the sample. UV-exposure (20min) resulted in death of individual cells within 2h, while surrounding cells remained healthy.

Single cell ablation and junction cutting

Cell ablations and intercellular junction cutting were carried out using a Chameleon-XR Ti-sapphire laser coupled to a Zeiss LSM510Meta upright confocal microscope. Cells were ablated by scanning 890nm laser light over a 9x9 pixel ROI (0.28µm² pixels) at 100% laser power (63mW nominal) and dwell time of 3.2µs.pixel⁻¹ for 20 iterations, using a 40x 0.8NA objective. To cut junctions, 4x4 pixel ROIs, 20% laser power, 720nm

(12mW) and dwell time of $164\mu\text{s}\cdot\text{pixel}^{-1}$ were used.

Confocal imaging

Fixed samples were imaged using an inverted Zeiss LSM510Meta microscope, 63x oil objective (NA1.4) or a 20x objective (NA0.7). For live-imaging cells were placed in a heated chamber (37°C, 5% CO₂) on a spinning-disk confocal microscope (Ultraview-ERS, Perkin-Elmer, 40x oil objective (NA1.3). Z-stacks ($26\times0.7\mu\text{m}$) were recorded at 30 second intervals over 4-6 hours. In some experiments, $1\mu\text{g}/\text{ml}$ of propidium iodide was added to the imaging medium to identify permeabilized cells. For laser-ablations Z-stacks were acquired in 7 planes at $1\mu\text{m}$ separation at 30 second intervals.

Immunocytochemistry

For ZO-1 staining, monolayers were simultaneously fixed and permeabilised using a solution of: 1.75% paraformaldehyde, 1% sucrose, and 0.5% triton-X in PBS:DMEM at 37°C for 20min. For pMLC and RhoA staining, monolayers were fixed with a solution of 4% paraformaldehyde in DMEM at RT for 15min, and either exposed to acetone at -20°C for 5min (pMLC) or 0.5% Triton-X in PBS, 4°C for 5min (RhoA). Samples were incubated for 10min at 4°C in blocking solution ($10\text{ mg}\cdot\text{ml}^{-1}$ BSA in PBS) prior to incubation in primary antibodies. The following primary and secondary antibodies were used: anti-ZO1 (rabbit polyclonal, $2.5\mu\text{g}\cdot\text{ml}^{-1}$, Invitrogen), anti-pMLC (1:100 dilution, rabbit polyclonal, Cell Signalling), anti-RhoA-GTP ($5\mu\text{g}\cdot\text{ml}^{-1}$, mouse monoclonal, NewEast Biosciences), goat anti-mouse Alexa-Fluor647 and Alexa-488 ($10\mu\text{g}\cdot\text{ml}^{-1}$, Invitrogen), donkey anti-rabbit Alexa-Fluor568 ($10\mu\text{g}\cdot\text{ml}^{-1}$, Invitrogen). Phalloidin-Alexa488 (Invitrogen) or Atto-647 (Sigma) were used at 33-50nM and DAPI at $1\mu\text{M}$.

Inhibitors

The myosin-II inhibitor blebbistatin was added to the culture medium immediately after UV-exposure and left for the duration of the experiment. For live-imaging ruby-lifeact-MDCK cells were used (568nm excitation) to circumvent photo-inactivation/phototoxicity issues reported with blebbistatin at 488nm (Sakamoto et al., 2005).

Image processing and analysis

XYZT image-stacks were cropped into smaller regions ($50\mu\text{m}^2$) around individual cell death events using custom written Matlab routines. Each cell death event was then

examined in ImageJ using the View5D plugin (Rainer Heintzmann). Quantitative analysis was performed using Matlab. To generate kymographs the final image of actin ring closure was superimposed onto an image prior to ring formation (for **Figure 1b**, the image at 18min from **Figure S1a** was superimposed onto the image at 0min). A line was drawn through the centre of ring and intensity values along this line were plotted as a function of time (red line, left panel, **Figure 1b**). The time over which ring contraction took place was measured (in **Figure 1b**, between 120 and 140min) and the slopes of the movement of the junctions were used to calculate the speed and time taken for closure.

Quantification of changes in myosin activity

Quantification of changes in myosin activity was effected using Matlab routines. Briefly, the perimeter of the dying cell was manually drawn in the apical-junctional plane using the MRLC-GFP time-lapse images (or brightfield images) for time-points separated by 2min intervals starting from 10min prior to any observable movement of the cell junctions up until rosette formation. We assumed rosette formation was complete when the area of the dying cell in the confocal plane had decreased by 90%.

To measure the temporal evolution of the myosin intensity along the cell contour, we positioned ROIs (area $4 \mu\text{m}^2$) around the cell perimeter. The mean ROI intensity at each time-point was calculated for the z-plane of maximum myosin intensity. Background (mean intensity for an image plane below the coverslip) was subtracted for each data set. Time-series were smoothed with a running average of window-size 3.

Vertex model of tissue mechanics for MDCK-monolayers growing on a substrate

To model MDCK-monolayers growing on a substrate, we adapted an existing computational model of drosophila epithelium (Marinari et al., 2012) based upon previous vertex models (Farhadifar et al., 2007; Kafer et al., 2007). It uses the following work function W :

$$W = \sum_{\alpha} \frac{K}{2} (A_{\alpha} - A_0)^2 + \sum_{\langle i,j \rangle} 2\Lambda l_{ij} + \sum_{\alpha} \frac{\Gamma}{2} L_{\alpha}^2$$

The first term in the work function reflects an area constraint where K_{α} is the effective bulk modulus, A_{α} the current area and A_0 the preferred area of a cell α . The second and third terms have a certain degree of redundancy. The second term represents a line tension acting along the length of a junction l connecting vertices i and j reflecting the balance of intercellular adhesion and cortical tension. The third term represents the actomyosin

contractility Γ acting around the cell perimeter L_a due to forces acting along the intracellular actin belt present at adherens junctions. We showed uniform localization of myosin at the cell cortex throughout apical contraction and reasoned that a tension applied to the entire perimeter of the cell was sufficient to reflect the mechanical contribution of cortical myosins and thus cortical tension could be represented by Γ alone and that Λ was only due to intercellular adhesion.

The energy of the system is minimised via random sampling, using a Monte Carlo method. The probability of a vertex move being accepted or rejected depends on the associated energy change in the work function: if the move decreases the energy of the system, we accept the move: $\Delta W < 0$, $P=1$; if the move does not change the energy of the system, the move is accepted with a probability of 0.5: $\Delta W = 0$, $P=0.5$; if the move increases the energy of the system, the move is rejected: $\Delta W > 0$, $P=0$.

We undertook a thorough calibration to choose parameters K , Λ , and Γ representative of our experimental conditions (rather than the original *Drosophila notum*). This involved running simulations to find the parameter set best able to replicate experimental data used for calibration.

To probe the mechanical properties of the system, we used laser-ablation to cut individual intercellular junctions. By comparing the movement of the vertices of the cut junction to simulations, it was possible to calibrate the relative magnitudes of model parameters Λ and Γ (Farhadifar et al., 2007). Following ablation, the vertices of the cut junction moved apart from one another. Simultaneously, the perimeters of the two cells expanded a small amount. Equilibrium was reached within 40-140s. The length change of the cut junction and the area and perimeter changes for the two cells linked by the cut junction were measured (9 cuts, 3 experiments): junction length increased by $1.0 \pm 1.0 \mu\text{m}$, while cellular perimeter increased by $2.5 \pm 2.5 \mu\text{m}$ (average perimeter: $9 \pm 4 \mu\text{m}$), suggesting that junction cutting affects both Λ and Γ . If only Λ for the cut junction was affected, the absolute increase in cell perimeter should be the same as the change in junction length. However, the perimeter of both cells increased by a length 2.5-fold greater than the increase in junction length, suggesting that Γ was also affected. The outward movement of the vertices showed that junctions were under positive line tension. To numerically simulate junction cutting, a random junction was chosen from an equilibrium configuration of the tissue. For that junction, adhesion Λ and contractility Γ were set to zero for the two cells

linked by the cut junction, as in Farhadifar et al. (2007). The other parameters remained unchanged. The change in the ‘cut’ junction length was then calculated.

In addition, we performed experiments in which we ablated a single cell. Following ablation, the area change was measured in the targeted cells and compared to simulations to estimate the relative magnitudes of K and Γ . Laser-ablation caused outward recoil of the surrounding cell junctions that relaxed over a period of ~ 140 s and the ablated cell’s area increased by $15 \pm 10\%$ (12 cells, 3 experiments). Laser ablation damaged the target cells and we assumed that this decreased cellular elastic modulus due to permeabilization and perturbation of the cell (**Figure 5**). The outward junctional movement suggested that the targeted cell relinquished its pull on neighbouring cells, and therefore that both Γ and \mathcal{A} were affected by ablation. Since some cellular remnants were still present following ablation, we assumed that cellular elasticity K and adhesion energy \mathcal{A} were not reduced to zero. In our simulation of single cell ablation, a random cell was chosen from an equilibrium configuration of the tissue. For that cell, the effective bulk modulus K and the adhesion \mathcal{A} were set to half of their original values and the contractility Γ to zero. The change in the ‘ablated’ cell area was then calculated.

To calibrate the model, simulations were run to find the parameter set best able to replicate the experimental data gathered from analysis of cell packing, single junction cuts, and single cell ablations. The aim was to find a configuration representative of the principal forces acting across the monolayer which could then be used as the equilibrium starting point from which to simulate rosette formation during cell death. Our goal was to generate an equilibrium configuration with mechanical properties that could replicate junction cutting, cell ablation experiments, and attain configurations that approximated observed MDCK-cell packing.

Simulations were run varying: \mathcal{A} , Γ , K and the amount of compression applied to the monolayer (Farhadifar et al., 2007). For each parameter set, the starting configuration was a network of 30 hexagonal cells of perimeter length $L = 6$. This was allowed to ‘grow’ for a specified number of cell divisions or time-steps. The resulting configuration was then used to simulate junction cutting and single cell ablation. The simulations were compared to experimental data using four criteria: 1) Δl_{cut} : the percentage length change in the cut junction. 2) ΔS_{cut} : the percentage area change in the cells linked by the cut junction. 3) ΔS_{ablate} : the percentage area change in the ablated cell. 4) ΔP : the sum of squared

deviations for the probability of n-sided cells (Gibson et al., 2006): $\Delta P = \sum_{n=3}^{\infty} (P_n^{sim} - P_n^{exp})^2$. The parameter set best able to replicate our experimental calibration data was $\frac{\kappa}{\Gamma} = 6$ and $\frac{\Lambda}{\Gamma} = -1.4$, after one round of cell division with the preferred area A_0 of daughter cells equal to that of mother cells. Numerical results are compared to experimental data in **Table 1**. Given that the model is a simplified description of an adherent MDCK-monolayer, we would not expect it to perfectly mimic experiments. In particular, simplifying assumptions made in generating the numerical model and in the boundary conditions chosen for junction cutting and ablation experiments may contribute to differences between numerical simulation results and experiments. However, with the optimal parameter set, our model was able to replicate all of the qualitative results of the calibration experiments as well as most of the quantitative results.

In Silico extrusion experiments

To investigate the respective role of the dying cell and its neighbours in the process of rosette formation, our code allowed us to separately specify the physical parameters for the dying cell (K_D , A_D , and E_D) and that of its immediate neighbours (K_N , A_N , and E_N). Using initial conditions in which monolayers had reached mechanical equilibrium, we carried out numerical experiments in which, at time $t=0$, we changed the physical properties of either the dying cell (to test mechanisms driven by a single dying cell, parameterized by A_D , E_D , K_D), of its immediate neighbours (to test mechanisms in which neighbours participated, parameterized by A_N , E_N , K_N), or both the dying cell and its immediate neighbours. The code was then run until it reached mechanical equilibrium and the area change of the dying cell was determined. Based on experimental observations, we defined rosette formation as resulting in a greater than 80% reduction in the apical area of the dying cell.

Acknowledgements

This article is dedicated to the memory of Professor Tom Duke who passed away suddenly during completion of this study. DK was part of the CoMPLEX Doctoral Training Program funded by EPSRC. GC was supported by a University Research Fellowship from the Royal Society. The authors thank Prof Buzz Baum, Dr Alexandre Kabla, and Dr Andrew Harris for careful reading of the manuscript.

References

- Andrade, D. and Rosenblatt, J.** (2011). Apoptotic regulation of epithelial cellular extrusion. *Apoptosis* **16**, 491-501.
- Bird, J. E., Daudet, N., Warchol, M. E. and Gale, J. E.** (2010). Supporting cells eliminate dying sensory hair cells to maintain epithelial integrity in the avian inner ear. *J Neurosci* **30**, 12545-56.
- Cai, Y. and Sheetz, M. P.** (2009). Force propagation across cells: mechanical coherence of dynamic cytoskeletons. *Curr Opin Cell Biol* **21**, 47-50.
- Charras, G. T., Hu, C. K., Coughlin, M. and Mitchison, T. J.** (2006). Reassembly of contractile actin cortex in cell blebs. *J Cell Biol* **175**, 477-90.
- Coleman, M. L., Sahai, E. A., Yeo, M., Bosch, M., Dewar, A. and Olson, M. F.** (2001). Membrane blebbing during apoptosis results from caspase-mediated activation of ROCK I. *Nat Cell Biol* **3**, 339-45.
- Eisenhoffer, G. T., Loftus, P. D., Yoshigi, M., Otsuna, H., Chien, C. B., Morcos, P. A. and Rosenblatt, J.** (2012). Crowding induces live cell extrusion to maintain homeostatic cell numbers in epithelia. *Nature* **484**, 546-9.
- Eisenhoffer, G. T. and Rosenblatt, J.** (2013). Bringing balance by force: live cell extrusion controls epithelial cell numbers. *Trends Cell Biol* **23**, 185-92.
- Fadok, V. A., Bratton, D. L., Frasch, S. C., Warner, M. L. and Henson, P. M.** (1998). The role of phosphatidylserine in recognition of apoptotic cells by phagocytes. *Cell Death Differ* **5**, 551-62.
- Farhadifar, R., Roper, J. C., Aigouy, B., Eaton, S. and Julicher, F.** (2007). The influence of cell mechanics, cell-cell interactions, and proliferation on epithelial packing. *Curr Biol* **17**, 2095-104.
- Gibson, M. C., Patel, A. B., Nagpal, R. and Perrimon, N.** (2006). The emergence of geometric order in proliferating metazoan epithelia. *Nature* **442**, 1038-41.
- Gu, Y., Forostyan, T., Sabbadini, R. and Rosenblatt, J.** (2011). Epithelial cell extrusion requires the sphingosine-1-phosphate receptor 2 pathway. *J Cell Biol* **193**, 667-76.
- Gu, Y. and Rosenblatt, J.** (2012). New emerging roles for epithelial cell extrusion. *Curr Opin Cell Biol* **24**, 865-70.
- Hogan, C., Dupre-Crochet, S., Norman, M., Kajita, M., Zimmermann, C., Pelling, A. E., Piddini, E., Baena-Lopez, L. A., Vincent, J. P., Itoh, Y. et al.** (2009). Characterization of the interface between normal and transformed epithelial cells. *Nat Cell Biol* **11**, 460-7.
- Kafer, J., Hayashi, T., Maree, A. F., Carthew, R. W. and Graner, F.** (2007). Cell adhesion and cortex contractility determine cell patterning in the *Drosophila* retina. *Proceedings of the National Academy of Sciences of the United States of America* **104**, 18549-54.
- Kim, K. S., Cho, C. H., Park, E. K., Jung, M. H., Yoon, K. S. and Park, H. K.** (2012). AFM-detected apoptotic changes in morphology and biophysical property caused by paclitaxel in Ishikawa and HeLa cells. *PLoS One* **7**, e30066.
- Madara, J. L.** (1990). Maintenance of the macromolecular barrier at cell extrusion sites in intestinal epithelium: physiological rearrangement of tight junctions. *J Membr Biol* **116**, 177-84.
- Marchiando, A. M., Graham, W. V. and Turner, J. R.** (2010). Epithelial barriers in homeostasis and disease. *Annu Rev Pathol* **5**, 119-44.

- Marinari, E., Mehonic, A., Curran, S., Gale, J., Duke, T. and Baum, B.** (2012). Live-cell delamination counterbalances epithelial growth to limit tissue overcrowding. *Nature* **484**, 542-5.
- Marshall, T. W., Lloyd, I. E., Delalande, J. M., Nathke, I. and Rosenblatt, J.** (2011). The tumor suppressor adenomatous polyposis coli controls the direction in which a cell extrudes from an epithelium. *Mol Biol Cell* **22**, 3962-70.
- Martin, P. and Lewis, J.** (1992). Actin cables and epidermal movement in embryonic wound healing. *Nature* **360**, 179-83.
- Mills, J. C., Stone, N. L. and Pittman, R. N.** (1999). Extranuclear apoptosis. The role of the cytoplasm in the execution phase. *J Cell Biol* **146**, 703-8.
- Potten, C. S. and Loeffler, M.** (1990). Stem cells: attributes, cycles, spirals, pitfalls and uncertainties. Lessons for and from the crypt. *Development* **110**, 1001-20.
- Riedl, J., Crevenna, A. H., Kessenbrock, K., Yu, J. H., Neukirchen, D., Bista, M., Bradke, F., Jenne, D., Holak, T. A., Werb, Z. et al.** (2008). Lifeact: a versatile marker to visualize F-actin. *Nat Methods* **5**, 605-7.
- Rosenblatt, J., Raff, M. C. and Cramer, L. P.** (2001). An epithelial cell destined for apoptosis signals its neighbors to extrude it by an actin- and myosin-dependent mechanism. *Curr Biol* **11**, 1847-57.
- Sakamoto, T., Limouze, J., Combs, C. A., Straight, A. F. and Sellers, J. R.** (2005). Blebbistatin, a myosin II inhibitor, is photoinactivated by blue light. *Biochemistry* **44**, 584-8.
- Sebbagh, M., Renvoize, C., Hamelin, J., Riche, N., Bertoglio, J. and Breard, J.** (2001). Caspase-3-mediated cleavage of ROCK I induces MLC phosphorylation and apoptotic membrane blebbing. *Nat Cell Biol* **3**, 346-52.
- Slattum, G., McGee, K. M. and Rosenblatt, J.** (2009). P115 RhoGEF and microtubules decide the direction apoptotic cells extrude from an epithelium. *J Cell Biol* **186**, 693-702.
- Tamada, M., Perez, T. D., Nelson, W. J. and Sheetz, M. P.** (2007). Two distinct modes of myosin assembly and dynamics during epithelial wound closure. *J Cell Biol* **176**, 27-33.
- Wang, J. and Pelling, A. E.** (2010). Cell sheet integrity and nanomechanical breakdown during programmed cell death. *Med Biol Eng Comput* **48**, 1015-22.

Table 1:

	Model	Data
% length change of cut junction	17 ± 13	17 ± 13
% area change of two cells joined by the cut junction	42 ± 12	20 ± 10
% area change of ablated cell	10 ± 7	15 ± 10

Table 1: Numerical results from Vertex model of tissue mechanics for MDCK-monolayers growing on a substrate compared to experimental data.

Figure Legends:

Figure 1. Removal of dying cells: a two-stage process consisting of apical contraction followed by extrusion.

(a) Confocal time-lapse images (individual Z planes) of UV-treated lifeact-GFP MDCK cells. Timings start 1 h 20 min after UV-treatment; xz and xy planes indicated by corresponding lines (green). Distances given for xy planes are measured from the basal-most plane; note the chosen xy plane is not the same for each time point. *0min*: No visible signs of actin activity or cellular shape changes were apparent. *15-30min* apical contraction and enclosure: an F-actin ring forms in the apical plane cleaving the apex of the dying cell and enclosing the basal part within the monolayer. *30min*: the apical junctions of the neighbouring cells have joined to make a rosette (arrow). **(b)** Kymograph revealing the dynamics of junctional closure (left panel). The kymograph was generated from time-lapse images shown in **Figure S1a**. Right panel, superimposed image of the cell junctions prior to closure and once closure was completed (see **Materials and Methods**). The red line indicates the location at which the kymograph was acquired. At t_1 , the junctions began moving at an approximately constant rate. At t_2 , the opposing junctions met and there appeared to be actin enrichment at the contact point. Time (min) after UV-exposure indicated. **(c)** Extrusion phase of the time-lapse sequence shown continued from (a). *45-7 min*: apical-lateral membranes of neighbouring cells move towards the basal plane and the dying cell is extruded. *75 min*: neighbouring cells crawl underneath the dying cell to heal the wound. See [Movie 1](#) for entire time-lapse sequence. Scale bars, 10µm. **(d)** Schematic diagram depicting the cellular events underlying apical contraction, enclosure and extrusion.

Figure 2. Cell membranes permeabilise after extrusion not before.

Confocal images from 3-D time-lapse movies of UV-treated lifeact-GFP MDCK cells. Propidium iodide (PI) and Annexin V-Alexa633 were included in the medium to reveal membrane permeabilization to reveal the appearance of phosphatidylserine (PS) on the outer leaflet of the plasma membrane. **(a)** Time-lapse series **0 to 15min**: during the initial apical contraction and rosette formation phase, no PI/PS fluorescence can be seen indicating that the membrane of the dying cell (*) was not compromised. At 15 min a rosette has formed enclosing the dying cell (arrow). **30 min**: the dying cell is extruded and PS (blue) can be seen as the cell leaves the monolayer (arrow). **(b)** PI and annexin staining in extruded cells at the monolayer apical surface. Left panel: on the monolayer surface,

extruded cells can be seen labelled with both PI and annexin (arrows). Right panels: boxed regions from left panel. The cell has been fully extruded and its neighbours form a continuous layer beneath it (arrow in the lower, xz panel), indicating that the extrusion phase is complete. Green lines in each image indicate the location of the xz and xy images. Scale bars, 10µm in a/ b (right panels), 50µm in b (left panel).

Figure 3. An actin ring in the dying cell drives apical contraction, enclosure and rosette formation whereas an actin ring in the neighbouring cells drives extrusion.

(a) Cellular mosaics of lifeact-GFP (green) and actin-mRFP (red) MDCK cells. Boxes indicate areas shown in b and c. (b) Extrusion of a dying cell (GFP) surrounded by 4 mRFP cells (GFP shown only). Actin activity is observed in two distinct planes within the dying cell. Apically (top sequence, line A in xz) an actin ring (arrow) contracts and cleaves the dying cell's apex. Basally (middle sequence, line B in xz), the dying cell retracts from the substrate. Times are from 2h 20min after UV-exposure. See [Movies 3 and 4](#). (c) Dying cell (mRFP) surrounded by 3 GFP cells (GFP shown only). Surrounding cells spread to enclose the dying cell within the monolayer (apical sequence, line A in xz), see [Movie 5](#). Basally, no signs of migration to close the wound (basal sequence, line B in xz). Times are from 2h 12m after UV-exposure. (d) XZ profile, F-Actin activity in a cell adjacent to a dying cell (*) during apical contraction and enclosure; time (mins), from 1h 50min after UV-exposure. Apical contraction and enclosure occurs between 5 and 40min with no obvious actin enrichment in neighbouring cells during this phase. Extrusion occurs at 45-60 min; F-Actin enrichment initially at apical contact between surrounding and dying cell, moves basally as extrusion progresses. Finally, adjacent cell crawls beneath dying cell to close wound. See [Movie 6](#) (GFP and mRFP) and [7](#) (GFP alone). Scale bars, 20µm for a and 10 µm for b, c and d.

Figure 4. An intracellular F-actin ring forms during the apical contraction phase and an intercellular F-actin ring forms during the extrusion phase.

MDCK cells fixed 2h (a) and 2.5h (b) after UV-exposure. (a) Apical contraction phase: cell appears to be in the process of apical cleavage by an F-actin ring in the plane of the tight junctions. The nucleus displays signs of condensation characteristic of cell death. The line scan (for far right image) reveals that F-actin enrichment (red line) is contained within the ZO-1 expression (green line), indicating that the F-actin ring is contained within the dying cell. (b) Extrusion phase: the condensed nucleus indicates a late apoptotic

cell. The nucleus of the dying cell is apical to that of its healthy neighbours and F-actin enrichment appears below and around the dying cell, indicating extrusion. Line scan (for far right image) reveals that F-actin enrichment (red line) is external to the ZO-1 staining (green line), indicating that the F-actin enrichment is due to an *intercellular* F-actin ring in the surrounding cells. All colour-merged images show F-actin (red), tight junctions labelled with anti-ZO-1 (green) and nuclei stained with DAPI (blue). The position of the xy images (1 and 2) are indicated by green lines in the lower xz images. Scale bar for (a) and (b), 10µm.

Figure 5. Cell death via laser-ablation induces the formation of an intercellular F-actin ring in neighbouring cells.

Time-lapse sequence of lifeact-GFP MDCK cells before and after laser ablation of the central cell (*). Green lines indicate locations of the corresponding xz and xy profiles. Distances given are measured from the basal-most plane and indicate the shift in position of the xy plane displayed. **0min**: immediately after ablation, fluorescence decreases in the cytoplasm of targeted cell, indicating cell permeabilization. Concurrently, junctions with adjacent cells move outwards (estimated increase in surface area of the ablated cell ~10%). **10-25min**: an actin ring forms at the apical junctions of neighbouring cells. It contracts and moves towards the basal plane, as described previously (Tamada et al., 2007). **30 to 40min**: the actin ring reaches the basal plane and the neighbours join to form a rosette. Scale bar, 10µm.

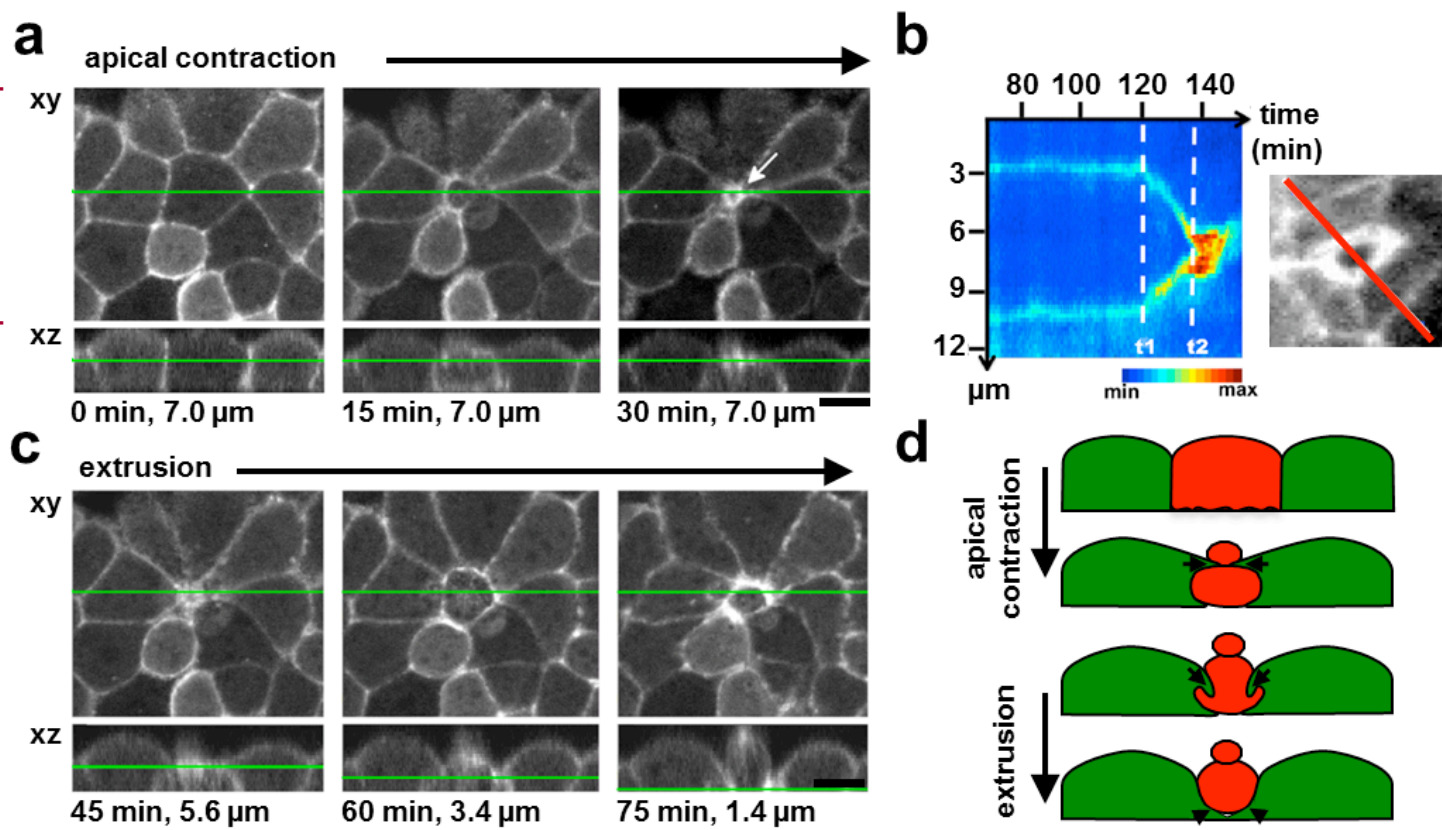
Figure 6. Myosin activity is required for rosette formation, apical contraction and enclosure. (a) Myosin accumulates at the site of the actin ring during apical contraction and rosette formation. Time-lapse sequence of MRLC-GFP MDCK cells, from 2h 40min after UV-exposure. Initially MRLC-GFP localization is diffuse with some enrichment at focal adhesions. At 5-20min apical contraction of the dying cell is observed. Myosin enrichment is seen around the periphery of the dying cell and is visible in the form of a myosin ring, see [Movie 8](#). **(b)** Single confocal section of a dying cell during the apical contraction phase labelled with anti-phosphorylated myosin light chain (pMLC, green), F-actin (red) and nucleic acids (blue). The dying cell (arrow) is enriched in pMLC. Zx images are displayed below; the location of xy and zx profiles are indicated by green lines. **(c)** Time-lapse images of a dying cell in the presence of 10 µM blebbistatin (ruby-lifeact

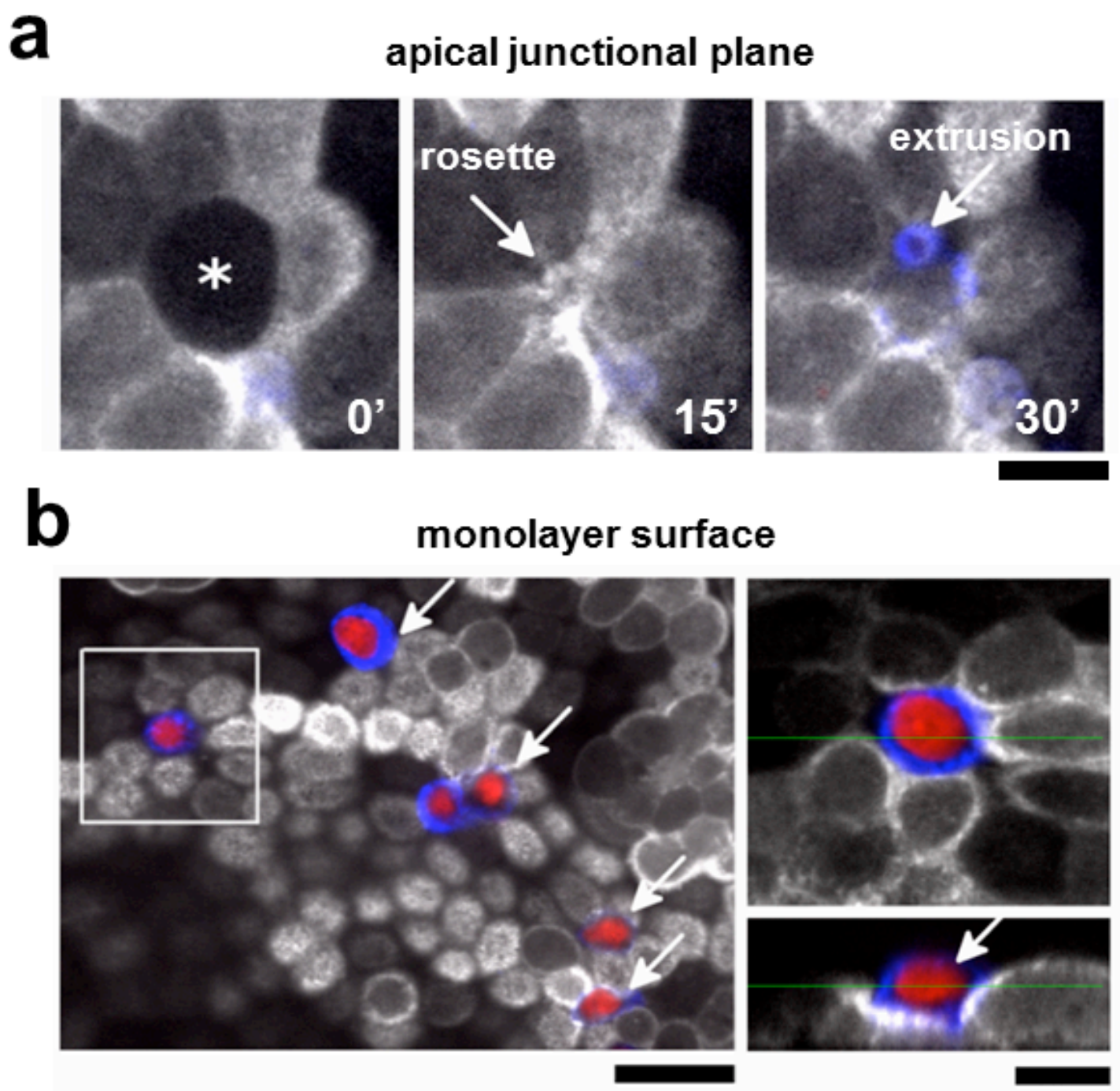
MDCK cells) show apical contraction is incomplete in the presence of low concentrations of the myosin inhibitor. At **0min**: no evidence of F-actin activity or shape change. **17-34min**: an actin ring forms and contracts in the apical plane. **34-51min**: having reached $\sim 1/3$ of its initial diameter, ring closure stalls, the dying cell ruptures, and surrounding cells relax back to their initial positions, see [Movie 9](#). **(d)** At higher concentrations (100 μM), blebbistatin prevents apical contraction. Images of a dying cell (*) which shows no inward contraction yet ruptures at $\sim 40\text{min}$. Overlays of the first (green) and last (red) images in the sequence reveal outward movement of the surrounding cells upon central cell rupture. In the basal plane, the healthy surrounding cells extend lamellipodia beneath the dying cell to heal the wound via crawling. Time indicated from 2h 15min after UV-exposure. Scale bar, 10 μm .

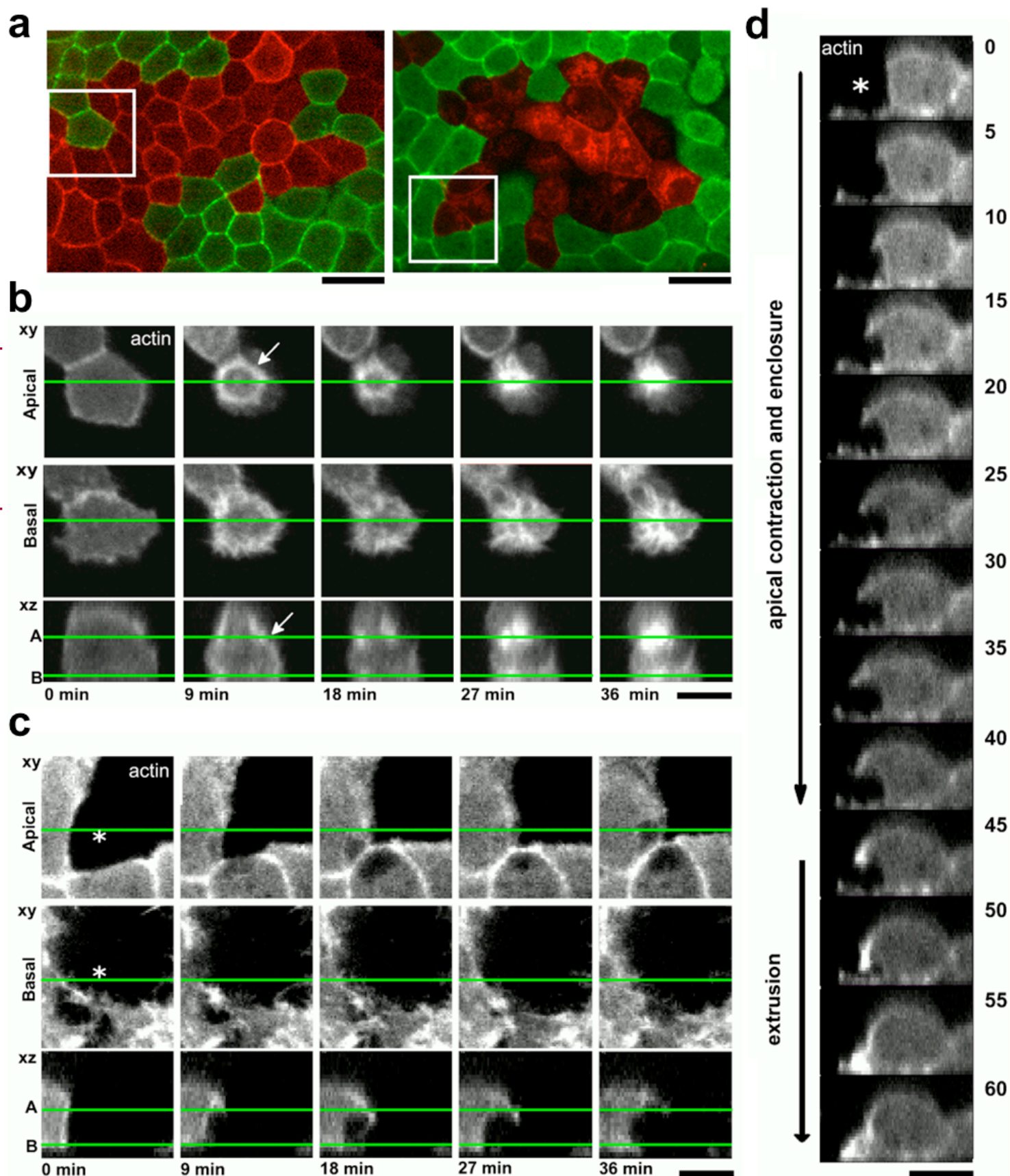
Figure 7. Rho-mediated contractility in the dying cell is necessary for apical contraction and rosette formation. **(a)** Single confocal sections (top panels) showing a dying cell during the apical contraction phase labelled for active RhoA (RhoA-GTP, green), F-actin (red), and nucleic acids (blue). Lower panels, xz images at the position indicated by the green lines. The dying cell (arrow) is enriched in RhoA-GTP at its apex (see xz profile). **(b-c)** Time-lapse images of UV-exposed mosaics of lifeact-GFP (green) and RhoGAP-mcherry (red) MDCK cells. In **(b)** a dying lifeact-GFP cell (*) undergoes F-actin ring closure and apical scission despite having RhoGAP-mCherry neighbours (3 of 5 cells) that are unable to contract. Note, GFP-only shown in greyscale panels. Upper xy panels: actin ring is not localised in a single plane and in xz (lower panels) it appears tilted (left side higher than the right side, arrows). See [Movie 10](#). **(c)** A dying RhoGAP-mcherry cell cannot drive apical contraction and rosette formation. First panel, dying cell (*) and its neighbours, two of which are lifeact-GFP cells (green) and two are RhoGAP-mCherry (red). At **0-27min**: cell borders adjacent to the dying cell move inwards. **36min**: apical contraction fails and cells move away from one another. **45+min**: F-actin at the apical membranes of neighbouring cells, which crawl basally around/under the dying cell (see xz panels). See [Movie 11](#). Times are from 2h 10min after UV-exposure. Scale bar, 10 μm .

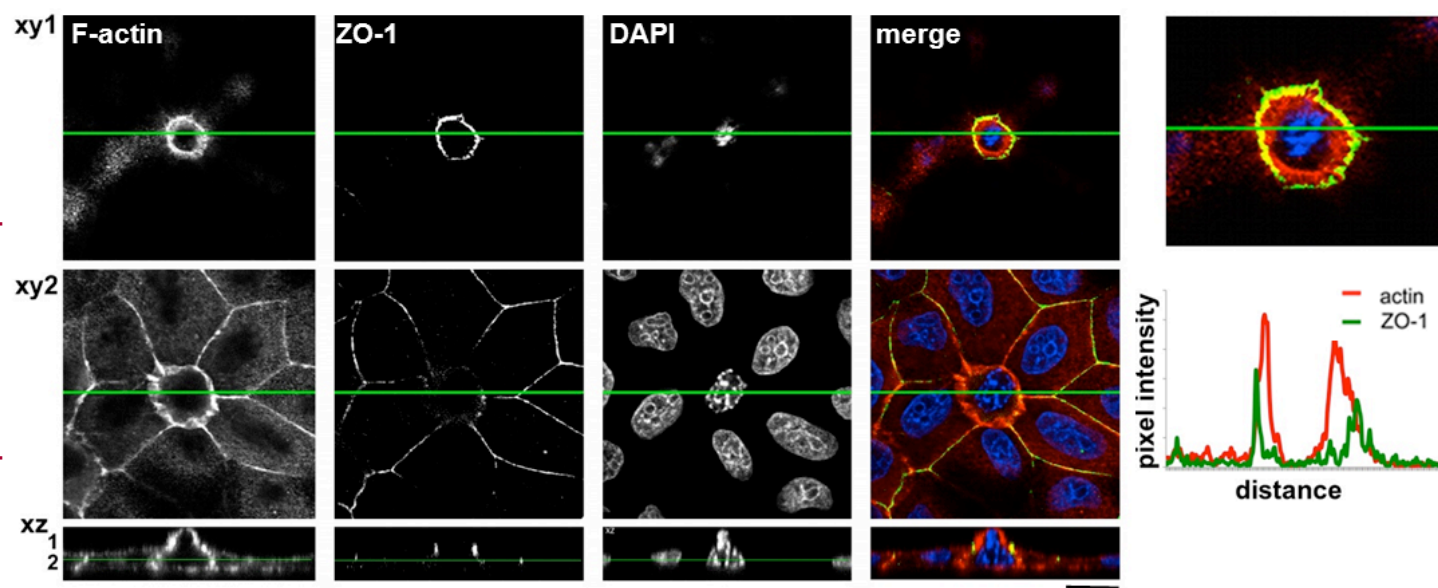
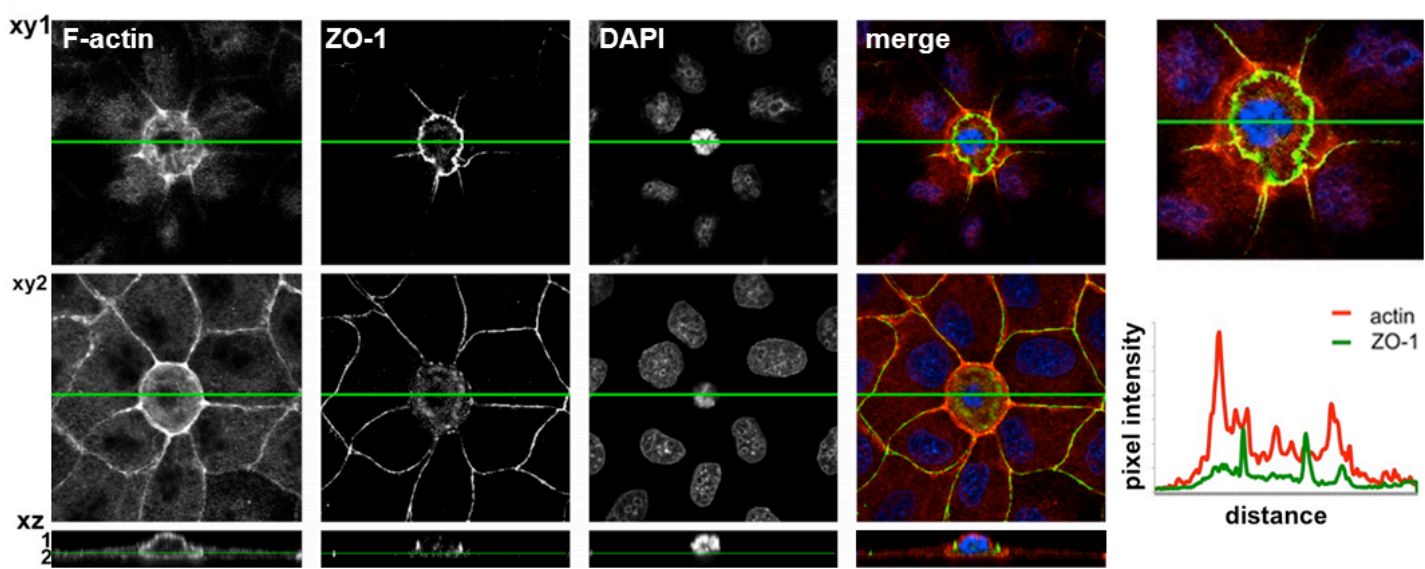
Figure 8. Numerical simulations indicate increased myosin contractility in the dying cell is sufficient to drive rosette formation. **(a)** Representative images of monolayers from computational model before perturbation and at equilibrium following changes of a

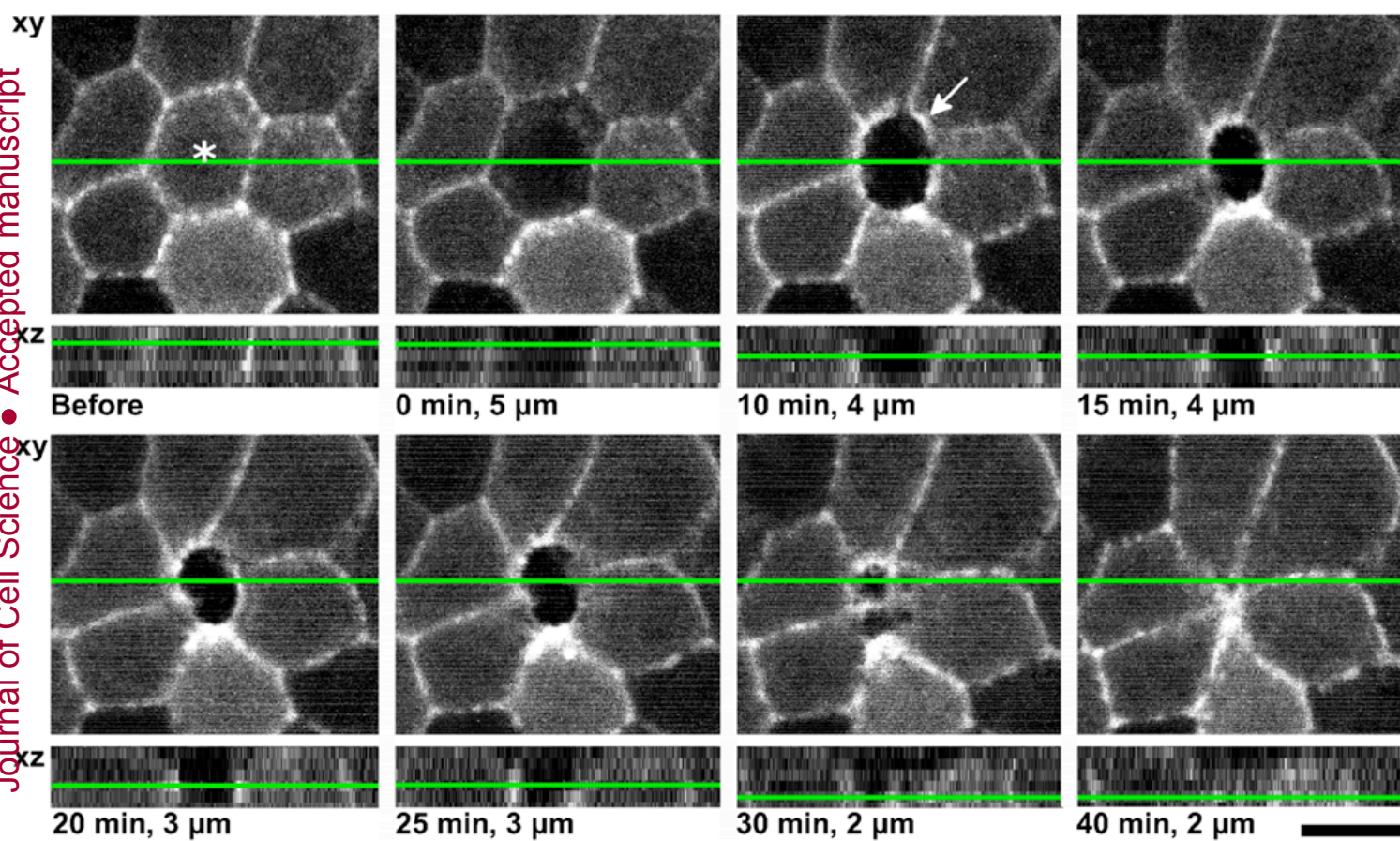
single parameter (indicated) in the dying cell (yellow). **(b)** Area reductions for different sets of parameter changes in simulations. Dotted line, rosettes considered formed for reductions $>80\%$. **(c)** Conceptual model of cell removal following death due to UV-exposure and laser ablation. **UV-exposure:** both the dying cell and its neighbours are involved in driving epithelial repair in a two-stage process: apical contraction and enclosure in the monolayer followed by extrusion. a: Enclosure initiates with formation of an actomyosin ring in the apical-junctional plane of the dying cell (red). b,c: Ring contraction draws in surrounding cells (green) in the apical plane, forming a rosette. Ring closure scissions the dying cell, leaving a portion on the apical surface. The majority of the cell is enclosed within the monolayer below the rosette. Coincident with junctional closure, the dying cell detaches from substrate. d: extrusion begins with formation of a multicellular F-actin ring in neighbouring cells. e: The intercellular actin ring moves basally to extrude the cell. f: Neighbouring cells heal basal area via crawling. **Laser-ablation:** Neighbouring cells heal the wound by closure of an intercellular F-actin ring combined with crawling along the substrate, mirroring the later phases (d-f) of cell removal following UV-exposure.

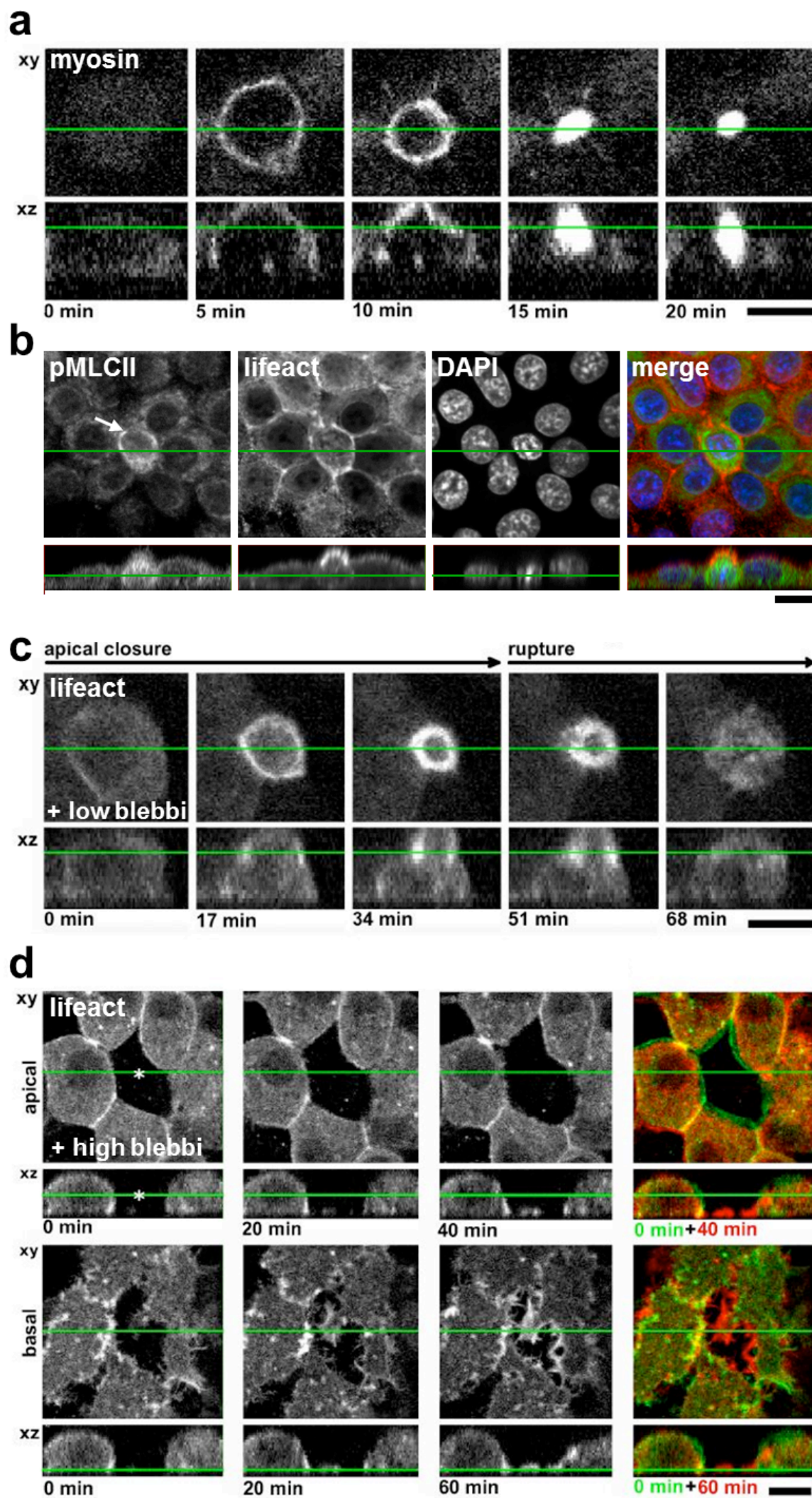




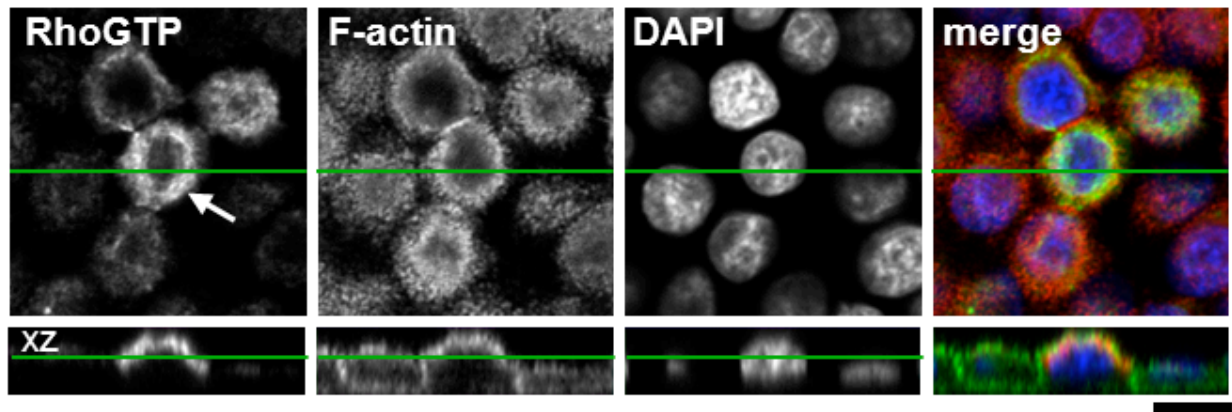


a**b**

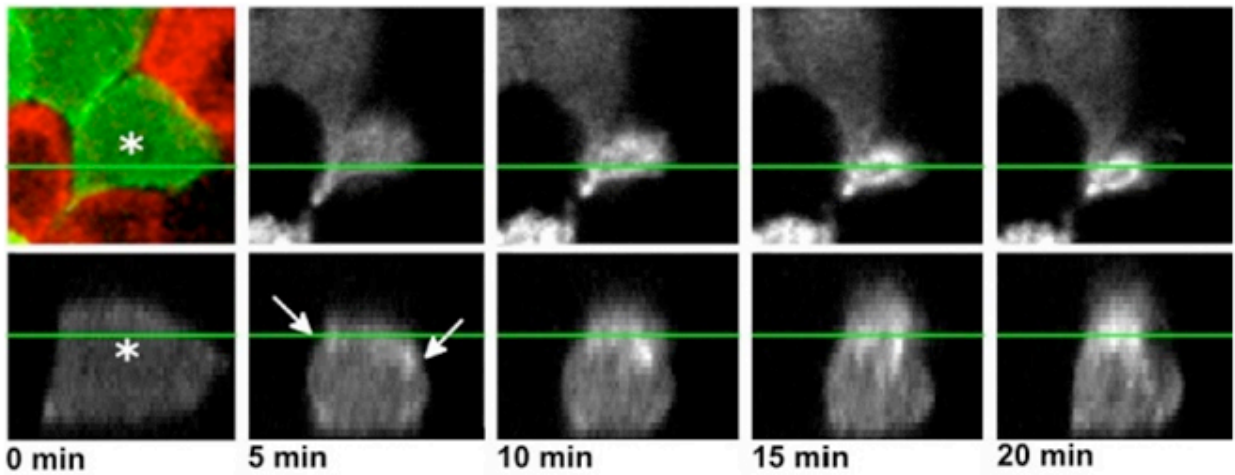




a



b



c

